A Quantum Chemistry Based Force Field for Perfluoroalkanes and Poly(tetrafluoroethylene)

Oleg Borodin,* Grant D. Smith, and Dmitry Bedrov

Department of Materials Science and Engineering and Department of Chemical and Fuels Engineering, 122 South Central Campus Drive, Room 304, University of Utah, Salt Lake City, Utah 84112

Received: May 22, 2002; In Final Form: July 25, 2002

An ab initio quantum chemistry investigation of conformational energetics of C_4F_{10}, C_5F_{12}, and C_6F_{14} revealed that the relative energies of gauche and ortho conformers relative to anti conformer were molecular weight independent for C_4F_{10}−C_6F_{14} whereas the gauche ↔ ortho and ortho ↔ anti barriers monotonically increased with increasing molecular weight. An ab initio quantum chemistry based force field has been developed for perfluoroalkanes and poly(tetrafluoroethylene) (PTFE). The same set of torsional parameters accurately described conformational energetics of C_4F_{10}, C_5F_{12}, and C_6F_{14} including gauche and anti splits, indicating transferability of the developed force field to longer perfluoroalkanes. Molecular dynamics (MD) simulations of various perfluoroalkanes ranging from C_4F_{10} to $C_{20}F_{42}$ using the developed force field yielded densities within 2% of experimental values, predicted enthalpies of vaporization within 10% of experimental data, and viscosities within 25% of experimental values. The static structure factor for C_9F_{20} at 295 and 373 K from MD simulations was found to be in excellent agreement with experimental X-ray measurements. The combined fraction of gauche and ortho conformers for C_5F_{12}−C_7F_{16} between 15% and 18% at 298 K predicted by the developed force field is in good agreement with the fraction of 19−24% from the analysis of D-LAM Raman bands of liquid perfluoroalkanes ranging from C_9F_{20} to $C_{20}F_{42}$ at 300 K. In contrast to the developed force field, the general OPLS-AA force field predicted a twice as low gauche fraction of only 7.2% for C_6F_{14}. The rotational isomeric state (RIS) model based on conformational populations of C_5F_{12} from MD simulations accurately reproduced the mean-square end-to-end distance for $C_{20}F_{42}$ for the developed force field and the OPLS-AA force field. The RIS model for the developed force field predicted a PTFE characteristic ratio of 15, higher than the value of 8 ± 2.5 from the light scattering experiments, whereas the general OPLS-AA force field yielded a much higher characteristic ratio of 28.

I. Introduction

Each year fluoropolymers enjoy additional new industrial applications. Perfluoroalkanes (PFAs) and poly(tetrafluoroethylene) (PTFE) are among the most technologically important fluoropolymers. Due to their chemical inertness, solvent resistance, extreme hydrophobicity, thermal stability, high lubricity, and low dielectric constant, PFAs and PTFE are excellent materials for coatings, sealants, surfactants, oxygen carriers, anesthetics and many other applications. Numerous theoretical and experimental studies of crystalline PTFE have been performed due to extensive industrial use of this polymer.[1] Relatively few studies have been conducted with the goal of understanding the amorphous phase of PTFE and its low molecular weight oligomers. A thorough understanding of the bulk and solution properties of PFAs becomes more significant due to increased industrial importance of liquid lubricants,[2] surfactant micelles,[3] mixed surfactants,[4] and fluorinated anesthetics.[5] Structural, conformational, and dynamical properties of PFAs as well as correlations between these properties are the most important factors determining the behavior of such systems. We believe that important progress in understanding PFA melts and solutions can be gained through a detailed molecular modeling study.

The paucity of simulation studies of liquid PFAs and their solutions is largely due to the absence of accurate force fields capable of describing the complex conformational characteristics of PFAs. The development and validation of accurate explicit atom force fields that properly reflect thermodynamic, structural, dynamic, and conformational properties of PFAs in bulk and solutions is the first step in simulation studies aimed at understanding the properties of PFA. These force fields should find immediate utilization among the modelers who investigate reverse micelles, surfactant monolayers, anesthetics, and many other systems whose behavior is greatly determined by local structure and chain conformations. A few force fields for PFAs have been reported in the literature,[6−10] but none of them provides an accurate description of the thermodynamic, structural, dynamic, and conformational properties of PTFE oligomers. Potentials derived by Holt and Farmer[6] showed a substantial improvement over previous force fields; however, the authors[6] concluded that further improvements were required in describing intermolecular interactions. A united atom force field by Cui el al.[7] yielded a good description of the vapor−liquid phase diagram of several PFAs[7] but significantly underpredicted their viscosities.[11] Despite excellent prediction of thermodynamic properties (densities and heats of vaporization) by the recently developed OPLS-AA force field,[10] this force field could not adequately describe conformational energetics of C_4F_{10} and C_5F_{12} using the same set of torsional parameters, thus bringing into question the transferability of the OPLS-AA force field to longer PFAs. Even when nontransferable torsional parameters were derived specifically for C_4F_{10} and C_5F_{12}, the

10.1021/jp026158i CCC: $22.00
Published on Web 09/04/2002

TABLE 1: Conformational Energies of Perfluorobutane Relative to the Anti Conformer[a]

level of theory	ref	gauche	g ↔ o	ortho	o ↔ a	anti	trans
MP2/D95+*//HF/D95+*	13	0.47		1.71		0	0.23
		(1.02)		(1.94)		(0)	(0.11)
MP2/D95+(2d)//HF/D95+*	13	0.49				0	0.19
		(1.03)				(0)	(0.14)
MP2/D95+(df)//HF/D95+*	13	0.38				0	
		(0.98)				(0)	
MP2/6-31G*//MP2/6-31G*	14	0.68		1.63		0	
		(1.21)		(2.0)		(0)	
MP2/6-311G*//MP2/6-31G*	14	0.85		2.12		0	
		(1.34)		(2.04)		(0)	
LMP2/cc-pvTz(-f)//HF/6-31G*	10, *a*	0.8	2.1	1.9	2.4	0	0.1
B3LYP/aug-cc-pvDz//B3LYP/aug-cc-pvDz	*c*	0.79	1.72	1.56	2.00	0	0.10
MP2/aug-cc-pvDz//B3LYP/aug-cc-pvDz	*c*	0.49	1.95	1.55	2.07	0	0.11
		(0.96)	(2.25)	(1.92)	(2.30)	(0)	(0.09)
MP2/aug-cc-pvDz//B3LYP/D95+*	*c*	0.49				0	
		(0.96)				(0)	
MP2/aug-cc-pvTz//B3LYP/aug-cc-pvDz	*c*	0.40				0	
		(0.97)				(0)	

[a] The Hartree−Fock energies are shown in parentheses. [b] Values obtained by spline fit to the LMP2/cc-pvTz(-f) energies taken at 10° intervals of C−C−C−C dihedral. [c] Present work.

force fields failed to predict a gauche split for both C_4F_{10} and C_5F_{12}.

As an accurate description of conformational energetics is critical for correct prediction of polymer dynamics as well as structure (e.g., chain dimensions), we initiated developing a quantum chemistry based force field that accurately describes conformational energetics of C_4F_{10}, C_5F_{12}, and C_6F_{14} with the same set of parameters, ensuring transferability of this force field to longer perfluoroalkanes. Our experience in developing polymer potentials based on ab initio studies of oligomers has revealed that the torsional parameters obtained from fitting conformational geometries and energies of smaller compounds are transferable to longer compounds of similar chemical structure.[12] In addition, we hoped to develop, in contrast to the OPLS-AA force field, a force field for PFAs without partial atomic charges, as simulations without long-range Coulomb interactions are significantly less computationally demanding.

The outline of this paper is the following: first, we describe ab initio quantum chemistry study of C_4F_{10}, C_5F_{12}, and C_6F_{14} with an emphasis on the molecular weight dependence of conformational energetics. In section III we develop an ab initio quantum chemistry based force field for PFAs based on the binding energy of a tetrafluoromethane dimer and the conformational geometries and energetics of C_4F_{10} and C_5F_{12} obtained from quantum chemistry and check the force field transferability to C_6F_{14}. Molecular dynamics (MD) simulation methodology together with the prediction of thermodynamic, conformational, dynamic, and transport properties of several PFAs (C_4F_{10}−C_9F_{20}) by MD simulations are presented in section IV. Structural properties, including a comparison with the static structure factor from X-ray measurements on C_9F_{20} are also presented in section IV. The comparison of structural, dynamic, transport, and thermodynamic properties predicted by our force field with those from the OPLS-AA force field is presented in section V.

II. Quantum Chemistry Studies of Conformational Energetics of C_4F_{10}, C_5F_{12}, and C_6F_{14}

A. Electron Correlation Effects. The majority of the previous quantum chemistry studies of PFAs have concentrated on perfluorobutane (PFB)[10,13,14] and perfluoropentane (PFP)[10,13] with a primary emphasis on the nature of trans and gauche splits and the gauche energy. Quantum chemistry results for perfluorobutane were recently summarized by Watkins and Jorgensen.[10]

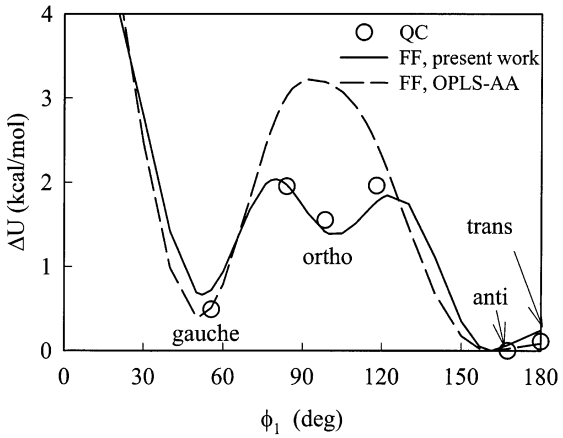

Figure 1. Relative conformational energies of C_4F_{10} as a function of the C−C−C−C torsional angle ϕ from ab initio quantum chemistry calculations at the MP2/aug-cc-pvDz//B3LYP/aug-cc-pvDz level (open circles show minima and barriers), the developed force field, and the general OPLS-AA force field.

In Table 1 we present only results from the previous studies with the largest basis sets, whereas Figure 1 shows conformer notation. Comparison of the gauche energy at the Hartree−Fock (HF) level with the calculations including Møller−Plesset correlation energy correction truncated at second order (MP2) indicates that MP2 gauche energies are approximately 0.4−0.6 kcal/mol lower than the corresponding HF gauche energy, indicating that inclusion of the correlation energy correction is important for an accurate description of conformational energetics of PFB.

B. Basis Set Size Effects. Table 1 shows that conformational energetics also depend on the quality of the basis set. The lowest gauche energy of 0.38 kcal/mol for PFB was obtained by Smith et al.[13] using single point energy calculations at the MP2 level with the standard double-ζ Dunning[15] basis set with a set of diffuse functions and a set of polarization d- and f-functions D95+(df) at the geometries optimized at the Hartree−Fock level using D95+* basis set (e.g., MP2/D95+(df)//HF/D95+* level). The highest gauche energy of 0.85 kcal/mol for PFB was obtained at the MP2/6-311G*//MP2/6-31G*[16] level by Albinsson et al.[14] The difference between those values is 0.47 kcal/mol, greater than the desired accuracy in conformational energies. Use of augmented correlation consistent polarized

TABLE 2: Torsional C−C−C−C Angle for the Perfluorobutane Conformers

level of theory	ref	gauche	g ↔ o	ortho	o ↔ a	anti	trans
HF/4-31G	13	57.1		98.5		169.4	180
HF/6-31G*	13	56	83	96	120	169	180
HF/D95+*	13	55.6		95.2		166.5	180
MP2/6-31G*	14	54.2		94.8		165.5	
B3LYP/D95+*	*a*	56.1			118.3	169.0	180
B3LYP/aug-cc-pvDz	*a*	55.6	83.6	95.5	118.7	167.5	180

[a] Present work.

valence basis sets (aug-cc-pvXz, X = D, T for double- or triple-ζ basis sets)[17] is preferred to standard split valence basis sets of 6-31G, 6-311G,[16] and D95[15] types used in the previous studies, as correlation consistent basis sets inherently have smaller basis set superposition errors that are impossible to correct intermolecularly. Our experience in the investigation of conformational energies of 1,2-dimethoxyethane revealed that MP2/aug-cc-pvDz energies at geometries optimized using density functional theory with the B3LYP[18] functional with an aug-cc-pvDz basis set provide conformational energies accurate to within 0.2−0.3 kcal/mol.[19] Therefore, we use aug-cc-pvXz type basis sets in this study.

C. Perfluorobutane. The Gaussian98 package[20] was used for all ab initio quantum chemistry calculations. Results of calculations for PFB are listed in Table 1 and Figure 1. To confirm that the basis set increase beyond aug-cc-pvDz does not significantly influence conformation energetics calculated at the MP2 level, we compared the gauche energy at the MP2/aug-cc-pvDz//B3LYP/aug-cc-pvDz level with that at the MP2/aug-cc-pvTz//B3LYP/aug-cc-pvDz level. Doubling of the basis set size (aug-cc-pvDz has 322 basis functions, and aug-cc-pvTz has 644 basis functions) decreased the gauche energy only by 0.09 kcal/mol, suggesting that a much smaller aug-cc-pvDz basis set is adequate for an investigation of conformational energetics of PFA. Table 1 also suggests that the B3LYP density functional energies generally agree better with the MP2 energies than the Hartree−Fock energies. We compared the MP2/aug-cc-pvDz energy differences for the gauche and anti conformers using geometry optimization done at the B3LYP/aug-cc-pvDz and B3LYP/D95+* levels and found the energies to be the same to within 0.01 kcal/mol and the C−C−C−C dihedral angle to differ only by 0.5° for the gauche conformer and 1.5° for the anti conformer, as shown in Table 2. Therefore we used the MP2/aug-cc-pvDz//B3LYP/D95*+ level for our investigation of conformation energetics of C_5F_{12} and C_6F_{14}. A more detailed examination of Table 2 also indicates that the C−C−C−C torsional angle agrees within 2° for all levels of theory listed except for HF/4-31G. The values of the C−C−C−C torsion for ortho and anti conformers at HF/4-31G differ from those at the MP2/6-31G* level by about 4°, ruling out HF/4-31G geometries from further studies of conformational energetics due to insufficient accuracy.

The zero-point energy contribution to the gauche conformer energy relative to the anti conformer was only 0.08 kcal/mol and therefore could be ignored in the analysis of conformational energetics.

D. Perfluorpentane and Perfluorohexane. Relative conformational energetics of C_5F_{12} at the MP2/aug-cc-pvdz//B3LYP/D95+* level as a function of the C−C−C−C dihedral ϕ_1 are shown in Figure 2a,b for two states of the other C−C−C−C dihedral ϕ_2 (anti and gauche). In these calculations the ϕ_1 dihedral was optimized in the case of minima and barriers or constrained for the intermediate geometries whereas all the other degrees of freedom were relaxed. Conformational energies

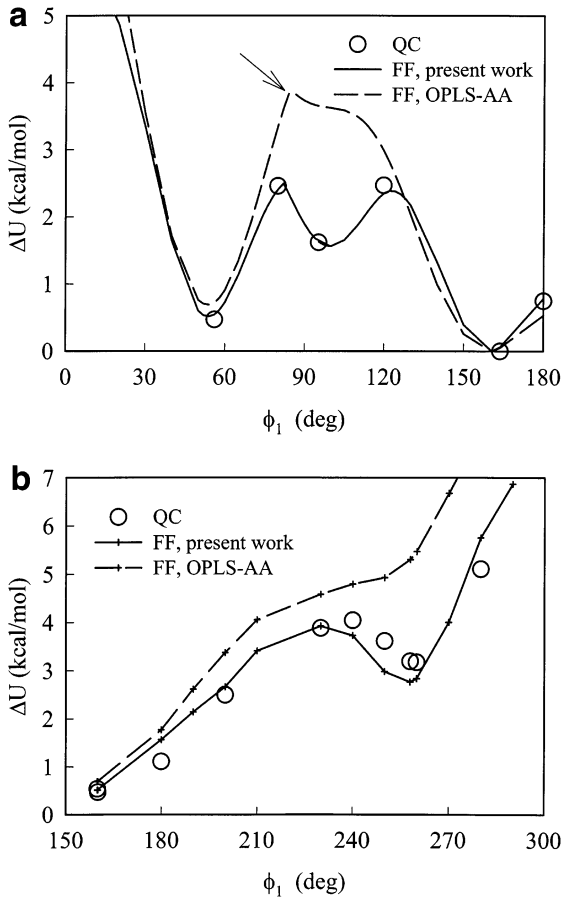

Figure 2. Relative conformational energies of C_5F_{12} as a function of the C−C−C−C torsional angle ϕ_1 with the angle ϕ_2 in the anti state (a) and the gauche state (b) from ab initio quantum chemistry calculations at the MP2/aug-cc-pvDz//B3LYP/D95+* level, the developed force field, and the general OPLS-AA force field. An arrow indictes the value of the ϕ_1 dihedral at which the ϕ_2 dihedral jumps from a^+ to a^-.

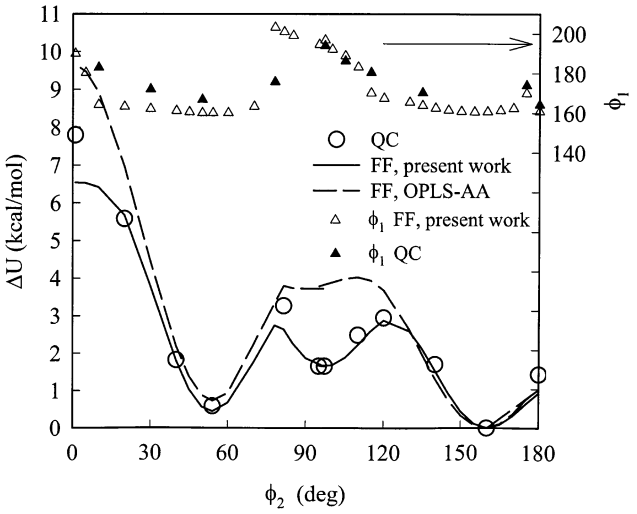

Figure 3. Relative conformational energies of C_6F_{14} as a function of the C−C−C−C torsional angle ϕ_1 with ϕ_2 and ϕ_3 in the anti state from ab initio quantum chemistry calculations at the MP2/aug-cc-pvDz//B3LYP/D95+* level, the developed force field, and the general OPLS-AA force field. The ϕ_1 angle corresponding to the ϕ_2 angle during the torsional drive is shown in the upper part of the graph.

of C_6F_{12} were calculated in a similar way and are shown in Figure 3. In these calculations the ϕ_1 and ϕ_3 C−C−C−C dihedrals were in the anti state but were not constrained. The

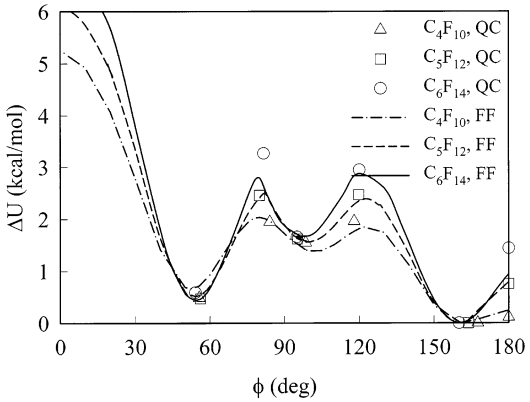

Figure 4. Relative conformational energies for the C_4F_{10}, C_5F_{12}, and C_6F_{14} conformers and barriers between them as a function of C−C−C−C torsional angle ϕ with the other C−C−C−C torsional angles in the anti state from ab initio quantum chemistry calculations at the MP2/aug-cc-pvDz//B3LYP/aug-cc-pvDz level for C_4F_{10} and MP2/aug-cc-pvDz//B3LYP/D95+* level for C_5F_{12} and C_6F_{14} (open circles indicate only minima and barriers) and the developed force field.

TABLE 3: Relative Energies (ΔU, kcal/mol) and Geometries (ϕ, deg) for the Representative Low-Energy Perfluorohexane Conformers from ab Initio Quantum Chemistry Calculations at the MP2/aug-cc-pvDz//B3LYP/D95+* Level and the Force Field

conformer	QC ΔU	FF ΔU	QC ϕ_1	QC ϕ_2	QC ϕ_3	FF ϕ_1	FF ϕ_2	FF ϕ_3
$a^-a^-a^-$	0.0	0.0	164.2	162.0	164.1	160.8	160.2	160.8
$a^-a^-g^+$	0.50	0.48	163.4	164.0	56.5	160.9	160.0	54.1
$a^-g^+a^-$	0.59	0.45	166.7	56.0	166.8	160.5	54.1	160.5
$a^+o^+a^+$	1.66	1.65	193.9	94.5	193.9	197.8	97.2	197.8
$a^+a^+o^+$	1.68	1.57	195.7	194.7	94.7	199.2	197.5	99.2
$g^+g^+a^-$	1.73	1.90	61.0	57.8	164.9	58.4	56.8	158.6

central C−C−C−C dihedral ϕ_2 was optimized in the case of minima and barriers or constrained for the intermediate geometries. Figure 4 summarizes the conformational minima and barriers for C_4F_{10}, C_5F_{12}, and C_6F_{14}, with all C−C−C−C dihedrals but the shown C−C−C−C dihedral ϕ being in the anti state. It is clear from Figure 4 that the gauche and anti splits exist for all molecular weights investigated, i.e., C_4F_{10}−C_6F_{14}. Further analysis of Figure 4 indicates that the torsional angle ϕ for the anti conformer decreases slightly from 169° to 162° with increasing molecular weight from C_4F_{10} to C_6F_{14}, whereas the position of the ϕ angle remains essentially the same for gauche and ortho for C_4F_{10}−C_6F_{14}. The positions of the g ↔ o, o ↔ a barriers slightly move away from the ortho minima with molecular weight increase. The relative energies of gauche, ortho, and anti conformers change very little with increasing molecular weight from C_4F_{10} to C_6F_{14}. The barrier (g ↔ o, o ↔ a, and trans) heights on the other hand monotonically increase with increasing molecular weight. Physical insight into this behavior will be obtained by using the force field parametrized in the next section.

Table 3 shows conformational energies and geometries of the representative low-energy perfluorohexane conformers. Examination of this table indicates that the $a^-g^+a^-$ conformer has an energy similar to that for $a^-a^-g^+$, indicating that the gauche energy is independent of the position of C−C−C−C dihedral within a chain; i.e., the gauche energy is essentially the same for the C−C−C−C dihedrals in the middle of the chain and for the C−C−C−C dihedrals at the chain ends. Likewise, the similarity of the conformational energies of $a^+o^+a^+$ and $a^+a^+o^+$ suggests that the ortho energy is also independent of the position of the C−C−C−C dihedral within the chain.

III. Force Field Development

A. Form of the Force Field and Development Methodology. In the classical force field developed below, the total potential energy of the ensemble of atoms, represented by the coordinate vector **r,** is denoted as $U^{tot}(\mathbf{r})$. The latter is represented as a sum of nonbonded interactions $U^{NB}(r_{ij})$ as well as energy contributions due to bonds $U^{BOND}(r_{ij})$ having bond length r_{ij}, bends $U^{BEND}(\theta_{ijk})$ having bending angle θ_{ijk}, and dihedrals $U^{TORS}(\phi_{ijkl})$ with dihedral angle ϕ_{ijkl} and is given by

$$U^{tot}(\mathbf{r}) = \sum_{i<j} U^{NB}(r_{ij}) + \sum_{ij} U^{BOND}(r_{ij}) + \sum_{ijk} U^{BEND}(q_{ijk}) + \sum_{ijkl} U^{TORS}(f_{ijkl}) \quad (1)$$

The nonbonded energy $U^{NB}(r_{ij})$ consists of the sum of two-body repulsion and dispersion energy terms between atoms i and j having atom types α and β represented by the Buckingham potential

$$U^{NB}(r_{ij}) = A_{\alpha\beta} \exp(-B_{\alpha\beta} r_{ij}) - C_{\alpha\beta}/r_{ij}^{6} \quad (2)$$

whereas contributions due to bonds $U^{BOND}(r_{ij})$, bends $U^{BEND}(\theta_{ijk})$, and torsions $U^{TORS}(\phi_{ijkl})$ for atoms i, j, k, and l having atom types α, β, γ, and δ, respectively, are given by

$$U^{BOND}(r_{ij}) = {}^1/_2 k_{\alpha\beta}{}^{BOND}(r_{ij} - r_{\alpha\beta}{}^0)^2 \quad (3)$$

$$U^{BEND}(\theta_{ijk}) = {}^1/_2 k_{\alpha\beta\gamma}{}^{BEND}(\theta_{ijk} - \theta_{\alpha\beta\gamma}{}^0)^2 \quad (4)$$

$$U^{TORS}(\phi_{ijkl}) = \sum {}^1/_2 k^t{}_{\alpha\beta\gamma\delta}(n)[1 - \cos(n\phi_{ijkl})] \quad (5)$$

where $r_{\alpha\beta}{}^0$ is an equilibrium bond length for atom types α and β; $\theta_{\alpha\beta\gamma}{}^0$ is an equilibrium bend angle for atom types α, β, and γ; and $k_{\alpha\beta}{}^{BOND}$, $k_{\alpha\beta\gamma}{}^{BEND}$, and $k^t{}_{\alpha\beta\gamma\delta}(n)$ are the bond, bend force constants, and torsional parameters. Nonbonded interactions are evaluated for all intermolecular atom pairs (ij) and for intramolecular atom pairs separated by three or more bonds.

The following force field development methodology is implemented. First, we determine the nonbonded parameters ($A_{\alpha\beta}$, $B_{\alpha\beta}$, and $C_{\alpha\beta}$) by fitting the repulsion parameters $A_{\alpha\beta}$ and $B_{\alpha\beta}$ to reproduce the complex energy of a perfluoromethane dimer at various geometries at the Hartree−Fock level. This level of theory does not include electron correlation effects that give rise to dispersion interactions described by the dispersion parameters $C_{\alpha\beta}$. Dispersion parameters are approximated by the London formula[21] using the dipole polarizability and ionization potential of carbon and fluorine atoms and then scaled by the same factor to match the density of C_7F_{16} liquid at 298 K, as described below.

At the next step of the force field development we fit the equilibrium bond length and bend angles (eqs 3 and 4) to obtain the best representation of the conformational geometries; the torsional parameters (eq 5) are fit to obtain the best representation of conformational energetics of C_4F_{10} and C_5F_{12}. Finally, the ability of the force field to predict conformational energetics of C_6F_{14} will be investigated.

B. Parametrization of Nonbonded Interactions. Quantum chemistry calculations of the perfluoromethane dimer at the Hartree−Fock level yield contributions to the complex energy primarily due to repulsion and electrostatic interactions. Per-

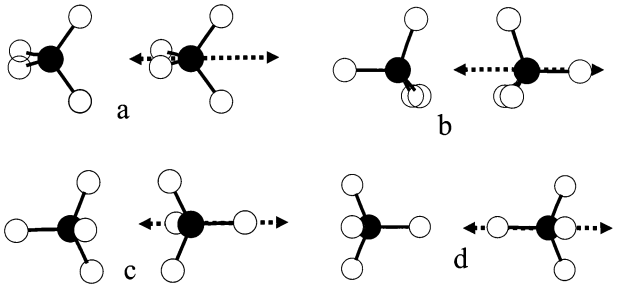

Figure 5. Geometries of $CF_4\cdots CF_4$ dimer.

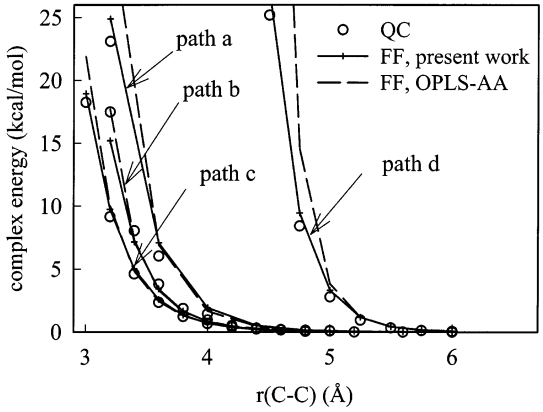

Figure 6. Complex energies as a function of separation for $CF_4\cdots CF_4$ dimer paths from Figure 5.

TABLE 4: BSSE-Corrected Complex Energy for Perfluoromethane Dimer at the Hartree−Fock Level at MP2/aug-cc-pvDz Geometry

basis set	complex energy (kcal/mol)	BSSE (kcal/mol)
aug-cc-pvDz	0.671	−0.49
aug-cc-pvTz	0.669	−0.18

fluoromethane has no net charge or dipole; thus a perfluoromethane dimer has only a relatively weak electrostatic interaction dominated by a quadrupole−quadrupole term, allowing us to approximate electrostatic and repulsion interaction by one set of the "effective" repulsion parameters ($A_{\alpha\beta}$ and $B_{\alpha\beta}$).

We investigated the effect of the basis set size on the complex energy of a perfluoromethane dimer at the Hartree−Fock level. The geometry optimization at the D_{2d} point group of a perfluoromethane dimer was performed at the MP2/aug-cc-pvDz level and is shown in Figure 5a. The single point energy calculations were performed at this geometry at the HF level using the aug-cc-pvDz and aug-cc-pvTz basis sets. The complex energy, defined as the energy of the complex minus the energy of each molecule at the complex geometry was calculated and is summarized in Table 4. The complex energies were corrected for the basis set superposition error (BSSE) using the counterpoise method.[22] The Hartree−Fock energy calculated using aug-cc-pvDz basis set is almost identical to that calculated with a much larger aug-cc-pvTz basis set, indicating that aug-cc-pvDz is sufficiently accurate for further calculations. The geometry optimizations were performed for the other complexes shown in Figure 5b−d at MP2/aug-cc-pvDz level. Then the paths shown in Figure 5 were generated by shifting one CF_4 along the line connecting C···C centers. The BSSE-corrected complex energies were calculated along each path and are shown in Figure 6.

The repulsion parameters (A_{F-F}, A_{C-F}, B_{F-F}, and B_{C-F}) were fit to reproduce the $CF_4\cdots CF_4$ complex energies and are shown in Figure 6, whereas A_{C-C} and B_{C-C} parameters were taken from our previously developed and tested force fields for poly(ethylene oxide)[23] and poly(vinylidene fluoride) (PVDF).[24] These parameters were initially derived by fitting crystal structures of poly(oxymethylene).[25] The resulting parameters are shown in Table 5. Figure 6 also shows the repulsion energies predicted by the OPLS-AA repulsion parameters for each path from Figure 5. The OPLS-AA repulsion energies agree well with the HF/aug-cc-pvDz energies for paths a−c for energies below 8 kcal/mol. For path d and for energies higher than 8 kcal/mol for paths a−c, the OPLS-AA force field predicts higher energies compared to quantum chemistry. Steeper repulsion is typical for the force fields using a Lennard-Jones repulsion term where the repulsion is proportional to $1/r_{ij}^{12}$.

TABLE 5: Nonbonded Force Field Parameters for PTFE

atom pair	A (kcal/mol)	B (Å^{-1})	C [(kcal Å^{-6})/mol]
F−F	63635.0	4.261	124.3
F−C	6923.2	3.084	315.8
C−C	14976.0	3.09	640.8

Initial dispersion parameters C_{F-F}, C_{F-C}, and C_{C-C} were approximated using the London dispersion formula[21] given by

$$C_{\alpha\beta} = -\frac{3}{2}\frac{IP_\alpha IP_\beta}{IP_\alpha + IP_\beta}\alpha_\alpha\alpha_\beta \qquad (6)$$

where IP_α and IP_β are the ionization potentials for atom types α and β and α_α and α_β are the polarizabilities of atom types α and β. $\alpha_C = 1.76$ Å^3, $\alpha_F = 0.557$ Å^3, $IP_C = 259.67$ kcal/mol, $IP_F = 401.78$ kcal/mol were used.[26] Preliminary MD simulation performed for C_7F_{16} using these nonbonded parameters, indicated that the density is approximately 25% below the experimental value at 298 K and 1 atm pressure. Therefore we scaled all dispersion parameters by 1.33 to match the density of C_7F_{16} for these parameters. Scaled dispersion parameters are given in Table 5.

C. Parametrization of Dihedral, Bending, and Bonding Interactions. At the next step of the force field development we determine parameters for bonding, bending, and dihedral interactions (eqs 3−5). The bending force constants ($k_{\alpha\beta\gamma}^{BEND}$) and bond force constant for the C−C bond (k_{CC}^{BOND}) were taken from the PVDF force field,[24] and the C−F bond force constant was fit to represent the distortion energy of one of the CF_4 bonds upon extension and compression at the B3LYP/aug-cc-pvDz level. The equilibrium bond length and bending angles were fit to yield the best description of equilibrium geometries of C_4F_{10} gauche, ortho, and anti conformation at the B3LYP/aug-cc-pvDz level and aa and ag conformers of C_5F_{12} obtained at the B3LYP/D95+* level. The valence force field parameters are summarized in Table 6.

The dihedral parameters for the F−C−C−F angle were obtained by fitting ab initio quantum chemistry energies for the CF_3-group rotation of C_4F_{10} at the MP2/aug-cc-pvDz//B3LYP/D95+* level (not shown). The dihedral parameters for the C−C−C−C torsion were determined to yield the best fit to the conformational energetics for C_4F_{10} and C_5F_{12} shown in Figures 1 and 2 as well as gg and go conformers of C_5F_{12}. Torsional parameters are given in Table 7. The quality of the fits is shown in Figures 1 and 2. Deviations of the force field relative conformational energies from the quantum chemistry values are within 0.2 kcal/mol for the most important conformers and barriers and 0.5 kcal/mol for the higher energy conformers and barriers. The ability of the developed force field to predict the rotational isomerization path for the central C−C−C−C torsion ϕ_2 for C_6F_{14} (with ϕ_1 and ϕ_2 being in anti state) is shown in

TABLE 6: Valence Force Field Parameters for PTFE[a]

bond type	K^{BOND} (kcal mol^{-1} Å^{-2})	r_0 (Å)
F−C_m	722.0	1.3391
F−C_e	722.0	1.3510
C_m−C_e	617.8	1.5658
C_e−C_e	617.8	1.5725

bend type	K^{BEND} (kcal mol^{-1} rad^{-2})	θ_0 (deg)
F−C_m−F	240.0	108.54
F−C−C	180.0	109.46
C−C−C	160.6	115.55
F−C_e−F	240.0	110.13

[a] C_m denotes a methyl carbon at the end group, C_e denotes all other carbon atoms, C denotes any carbon atom.

TABLE 7: Torsional Force Field Parameters for PTFE (kcal/mol)

type	k^t_1	k^t_2	k^t_3	k^t_4	k^t_5	k^t_6	k^t_7
C−C−C−C	−0.925	0.07	1.427	−0.540	−0.207	0.0	0.676
F−C−C−F	0.0	0.0	−0.380	0.0	0.0	0.0	0.0

Figure 3. The force field predicts the conformational energetics of the most important low-energy conformers of C_6F_{14} with an average error of 0.1 kcal/mol and a maximum error 0.2 kcal/mol from quantum chemistry values. The torsional angles of the low-energy conformers are predicted with an average error of 3.5°. The o ↔ a barrier is predicted within 0.1 kcal/mol, the trans and g ↔ o barriers are off by about 0.5 kcal/mol, and the high-energy cis barrier is off by about 1.2 kcal/mol. In general, we consider the description of the conformational energetics of C_4F_{10} and C_5F_{12} and predictions of conformational energetics of C_6F_{14} good.

Figure 3 shows changes of the first C−C−C−C dihedral ϕ_1 during a drive of the ϕ_2 dihedral from quantum chemistry calculations and the force field. Both quantum chemistry calculations and the force field predict a gradual decrease of ϕ_1 with changes of ϕ_2 from trans to anti. A further decrease in ϕ_2 from anti to ortho causes an increase in ϕ_1 with ϕ_1 crossing 180° around the a ↔ o barrier. Interpolation of quantum chemistry data in the region between ortho and gauche minima indicates a gradual decrease of ϕ_1 upon a ϕ_2 decrease from the ortho to gauche state, whereas the force field predicts an initial increase of ϕ_1 with an abrupt change of ϕ_1 from a^+ to a^- around ϕ_2 crossing the g ↔ o barrier. A further decrease of the ϕ_2 angle leads to an increase of ϕ_1 from both quantum chemistry and the force field. Again, we conclude that the force field is not only able to predict conformational energetics of C_6F_{14} but also to predict adequately conformational geometries.

We have finished development of the force field and are now in a position to use the force field to get insight into the molecular weight dependence of relative conformational energies from ab initio quantum chemistry calculations shown in Figure 4 and discussed above. The force field is able to describe the molecular weight dependence of conformational energetics well, as seen in Figure 4, and therefore can be used to get insight into the mechanism underlying this behavior. The main contributions to the relative conformational energies in our force field come from nonbonded terms eq 2 and torsional potential eq 5. The force field contributions to the total relative conformational energy for C_4F_{10} and C_6F_{14} from the nonbonded and torsional terms are shown in Figure 7. This figure illustrates that at all conformational minima (anti, ortho, and gauche) the relative nonbonded and torsional energies for C_4F_{10} are almost identical to those for C_6F_{14}. For the a ↔ o barrier the total energy

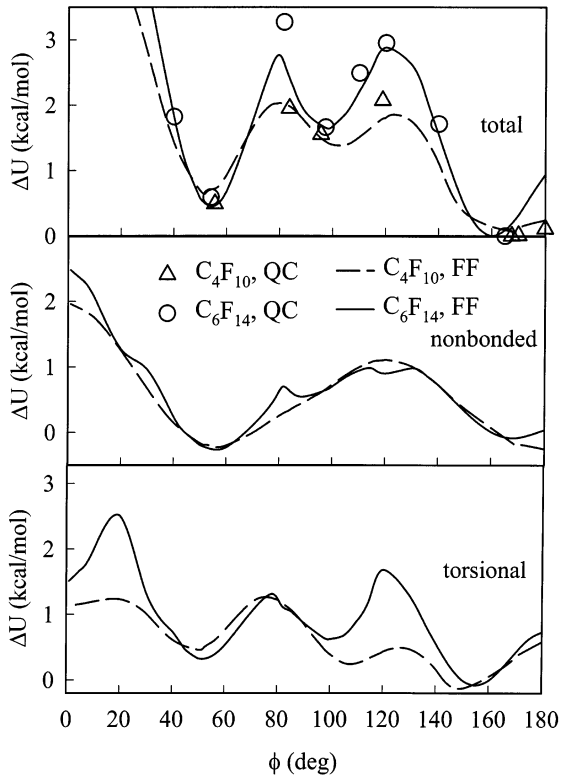

Figure 7. Relative conformational energies of C_4F_{10}, C_5F_{12}, and C_6F_{14} from ab initio quantum chemistry calculations and the force field.

is higher for C_6F_{14} than for C_4F_{10} for almost as much as the torsional energy, whereas the nonbonded energy is slightly less for C_6F_{14} than for C_4F_{10}, suggesting that the torsional potential is responsible for the increased barrier of C_6F_{14} compared to C_4F_{10}. An increase of the a ↔ o barrier with increasing molecular weight, on the other hand, is due to an increase of nonbonded contributions as well as a small contribution from the bending potential.

IV. Molecular Dynamics Simulations of Perfluoroalkanes

A. Simulation Methodology. MD simulations of C_4F_{10}, C_5F_{12}, C_6F_{14}, C_7F_{16}, C_9F_{20}, and $C_{20}F_{42}$ liquids were performed at the thermodynamic parameters given in Table 8 using the MD simulations code *Lucretius*[27] using the developed above force field. The Nose−Hoover thermostat and barostat[28,29] were used to control temperature and pressure. Dispersion interactions were truncated at 10 Å. An explicit reversible multiple time step integrator RESPA[29] with a time step of 0.75 fs for bonding, bending, and torsional motion, 1.5 fs for nonbonded interactions within 6 Å, and 3.0 fs for nonbonded interactions between 6 and 10 Å was used.

The systems were created in the gas phase, e.g., with a box size of 110−190 Å. The box was shrunk in MD simulations using a Brownian dynamics algorithm[30] for 1.5 ns to a box with linear dimensions 35−41 Å depending on a system approximately corresponding to the experimental density at 1 atm and 298 K for all systems except $C_{20}F_{42}$, where the density at 1000 atm was used because experimental data at 1 atm were not available. Then the systems were equilibrated at each temperature for 0.8 ns, followed by 1.0 ns NPT runs with unconstrained bonds. The average bond length during that 1.0 ns NPT run was calculated for each bond type and used in further simulations, in which the SHAKE algorithm[31,32] was employed to constrain bond lengths. The 2−3 ns NPT simulations were performed to obtain an equilibrium box size at

TABLE 8: Simulation Times (NPT+NVT Total Times), Densities (ρ), and Heats of Vaporization (ΔH) of PTFE Oligomers from MD Simulations with the Present Force Field and from Experiment at 1 atm for $C_4F_{10}-C_7F_{16}$ and at 1000 atm for $C_{20}F_{42}$[a]

compd	T (K)	trajectory length (ns)	ρ^{MD} (kg/m^3)	ρ^{exp} (kg/m^3)	ΔH^{MD} (kcal/mol)	ΔH^{exp} (kcal/mol)
C_4F_{10}	200	50	1785	1817		
C_4F_{10}	273	3	1569 (1581)	1600	5.92 (5.45)	5.46
C_4F_{10}	298	60	1507			
C_5F_{12}	215	5	1812	1853		
C_5F_{12}	298	30	1590 (1597)	1600	7.01 (6.52)	6.45
C_5F_{12}	318	3	1655	1652		
C_6F_{14}	298	35 (9)	1662 (1681)[a]	1675	8.36 (7.86)	7.51
C_7F_{16}	298	55	1710	1704	8.92	
C_7F_{16}	318	3	1655	1652		
C_9F_{20}	295	12	1769			
C_9F_{20}	377	4	1607			
$C_{20}F_{42}$	580	12 (10)	1744 (1752)	1726[c]		

[a] Values in parentheses are for the OPLS-AA force field. The experimental densities and heats of vaporization for all PFA but $C_{20}F_{42}$ were taken from the compilations by Watkints and Jorgensen.[10] [b] ρ^{MD}(OPLS-AA) = 1686 kg/m^3 was obtained in present MD simulations with Ewald summation. [c] Reference 33.

atmospheric pressure. Further simulations of the length given in Table 8 were performed in the NVT ensemble using the equilibrium box size at atmospheric pressure for all system but $C_{20}F_{42}$, where the density at 1000 atm was used. Atom coordinates were output every 1 ps for analysis, stress tensor was output every 9 fs.

Gas-phase simulations of C_4F_{10}, C_5F_{12}, and C_6F_{14} were performed to calculate average intramolecular energies using a Brownian dynamics algorithm.[30] Equilibrated systems were taken after the NPT runs of the corresponding simulations of liquids. Intermolecular interactions were turned off. The average energies were calculated during 2 ns runs after 0.2 ns equilibration.

B. Thermodynamic Properties of Perfluoroalkane. Densities of PFA oligomers from MD simulations with the developed force field are summarized in Table 8. The developed force field is able to predict densities of the PFAs simulated with an average error of 1% and with a maximum error of 2% from the experimental data[10,33] with a slight underestimation of densities of short oligomers at low temperatures and slight overestimation of the density of long oligomers at high temperatures. Heats of vaporization (ΔH) for the PFAs were calculated using eq 7 and are summarized in Table 8

$$\Delta H = U^{liq} - U^{vap} + RT \tag{7}$$

where U^{liq} and U^{vap} are the energies of liquid and gas phases, R is the gas constant, and T is temperature. Predicted by the developed force field, heats of vaporization are about 10% higher than the experimental values, which is an acceptable accuracy for many applications.

C. Conformational Properties. *Conformational Populations.* Figure 8 shows the C−C−C−C dihedral propability density for $C_4F_{10}-C_7F_{16}$ at 298 K. The C−C−C−C dihedral probability densities for C_5F_{12}, C_6F_{14}, and C_7F_{16} are very similar, whereas C_4F_{10} has a considerably higher probability of the ortho state and lower probability of the anti state and the gauche probability is only slightly higher than the one for C_5F_{12}, C_6F_{14}, and C_7F_{16}. These results are slightly different from those shown in Figure 4, which predicted that the gauche and ortho relative energies to the anti conformer are very similar for $C_4F_{10}-C_6F_{14}$ if all the other C−C−C−C torsional angles are in the anti state.

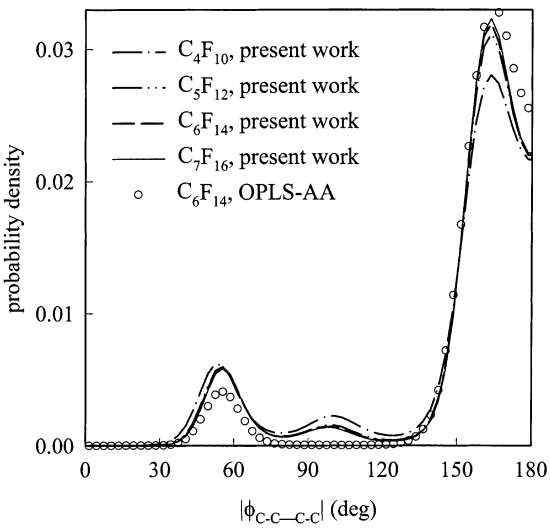

Figure 8. Probability density for the C−C−C−C angle for $C_4F_{10}-C_7F_{16}$ from MD simulations using the developed force field and for C_6F_{14} using the OPLS-AA force field at 298 K and 1 atm.

TABLE 9: Conformational Populations (%) of $C_4F_{10}-C_7F_{16}$ at 298 K from MD Simulations with the Developed Force Field[a]

compd	gauche	ortho	anti
C_4F_{10}	13.7	6.2	80.1
C_5F_{12}	10.9	5.2	83.9
C_6F_{14}	10.4	5.4	82.2
C_6F_{14}	(7.20)		(92.8)
C_7F_{16}	9.7	5.7	84.6

[a] Values in parentheses are for the OPLS-AA force field.

Therefore the difference is attributed to the neighboring torsions being in the gauche or ortho state.

To quantify the populations of the gauche, ortho, and anti conformers, we define the C−C−C−C dihedral ϕ being in the gauche state if $0° < \phi < 80°$ and $260° < \phi < 360°$, in the ortho state if $80° < \phi < 125°$ and $235° < \phi < 260°$, and in the anti state if $125° < \phi < 235°$. Populations of the gauche, ortho, and anti conformers for $C_4F_{10}-C_7F_{16}$ at 298 K are shown in Table 9. Consistent with Figure 8, the populations of C_5F_{12}, C_6F_{14}, and C_7F_{16} are similar, whereas for C_4F_{10} the population of the gauche state is higher and the anti population is lower than for the longer oligomers (C_5F_{12}, C_6F_{14}, C_7F_{16}). The MD simulations predict total populations of the gauche + ortho states for C_5F_{12}, C_6F_{14}, C_7F_{16} between 15 and 18%. Analysis of D-LAM Raman bands of liquid PFA from C_9F_{20} to $C_{20}F_{42}$ at 300 K indicates total populations of the gauche + ortho states being 19−24%.[34] This good agreement between current MD simulations and the Raman experiments provides an additional indication that the developed force field is capable of accurate representation of conformational energetics of PTFE oligomers.

Characteristic Ratio for PTFE. The characteristic ratio C_∞ of PTFE was calculated by parametrizing a previously developed six-state rotational isometric state (RIS) model[35] to reproduce the average conformational populations, average dihedral angles, and average C−C−C bending angle obtained from MD simulations of C_5F_{10} at 298 K with the developed force field. The RIS model was found to accurately reproduce the average end-to-end distance of $C_{20}F_{42}$ from MD simulations at 580 K and therefore was applied for prediction of C_∞, yielding a value of 15 at 600 K. This value is larger than the value of 8 ± 2.5 at 600 K obtained from light scattering experiments.[36] A possible reason for the higher characteristic ratio for PTFE from the MD-

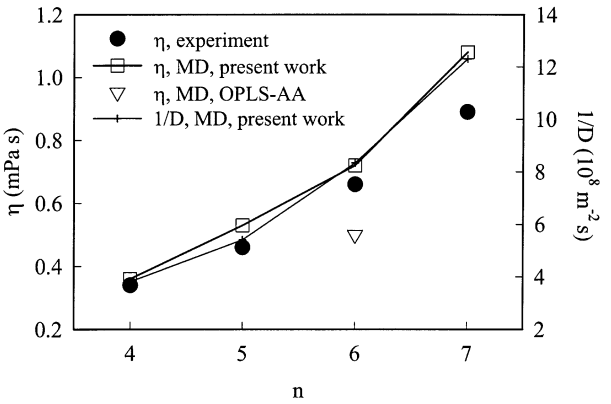

Figure 9. Dynamic viscosity and inverse self-diffusion coefficient for $C_4F_{10}-C_7F_{16}$ from MD simulations using the developed force field and for C_6F_{14} for the OPLS-AA force field at 298 K and 1 atm.

based RIS model compared to experiment is the somewhat lower gauche + ortho population found in PFAs in our simulations compared to D-LAM measurements, as discussed above. This appears to be due to a too low trans barrier predicted by the force field (compared to quantum chemistry as illustrated in Figure 3), which results in an increased fraction of the most extended a^+ and a^- conformers.

D. Transport Properties of Perfluoroalkanes. The viscosity η of many PFAs has been measured experimentally[37−40] and is accessible from MD simulations. The viscosity was calculated in MD simulations using the Einstein relation[41]

$$\eta = \lim_{t\to\infty} \frac{V}{20 k_B T t} \langle \sum_{\alpha\beta} (L_{\alpha\beta}(t) - L_{\alpha\beta}(0))^2 \rangle \qquad (8)$$

where $L_{\alpha\beta}(t) = \int_0^t P_{\alpha\beta}(t')\, dt'$, k_B is the Boltzmann constant, T is temperature, t is time, $P_{\alpha\beta}$ is the symmetrized stress sensor, and V is the volume of the simulation box. Viscosities of $C_4F_{10}-C_7F_{16}$ at 298 K from MD simulations together with the experimental viscosities[37−40] are shown in Figure 9. The viscosities from MD simulations are systematically higher than the experimental values but are still within 25% of the experimental values. Figure 9 also shows the self-diffusion coefficient for $C_4F_{10}-C_7F_{16}$ at 298 K. As expected, the inverse self-diffusion coefficient has a molecular weight dependence very similar to that of viscosity.

The dynamic viscosity was also calculated for C_4F_{10} at 200 K to check the temperature dependence of viscosity. The MD simulations yield $\eta^{MD} = 1.66$ mPa·s in good agreement with the $\eta^{exp} = 1.46$ mPa·s for C_4F_{10} at 200 K.

E. Comparison of the X-ray Structure Factor from Experiment and MD Simulations. The structure factor of C_9F_{20} was calculated through radial distribution functions using

$$H(k) = 1 + \frac{1}{\langle |f_\alpha|^2 \rangle} n \sum_{\alpha\beta} x_\alpha f_\alpha(k) x_\beta f_\beta(k) \int_0^{r_c} [g_{\alpha\beta}(r) - 1] \frac{\sin kr}{kr} 4\pi r^2\, dr \qquad (9)$$

where $\langle |f_\alpha|^2 \rangle \equiv \sum_\alpha x_\alpha f^2\alpha(k)$, n is a number density, $g_{\alpha\beta}(r)$ is the radial distribution function (RDF) for $\alpha\beta$ atom types, k is the wave vector, $f_\alpha(k)$ is the form factor for species α, x_α is a fraction of atom type α, and r_c is the cutoff for integration and was set to 16 Å. The structure factors for C_9F_{20} at 377 and 295 K from MD simulations using the developed force field and X-ray measurements[42] are shown in Figure 10. An excellent agreement

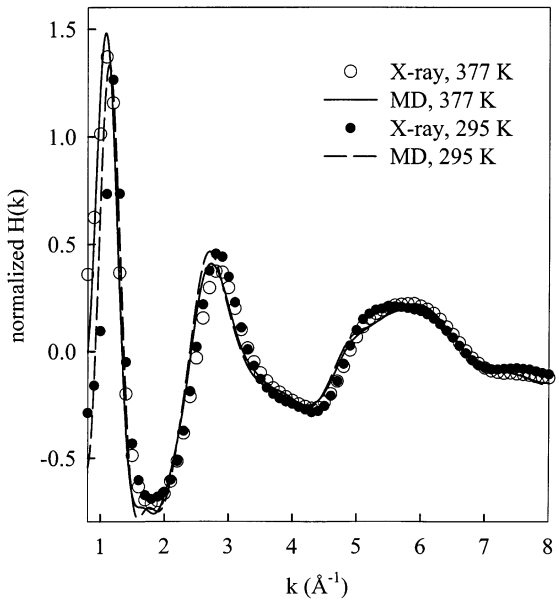

Figure 10. Static structure factor from X-ray measurements and MD simulations for C_9F_{20} at 1 atm.

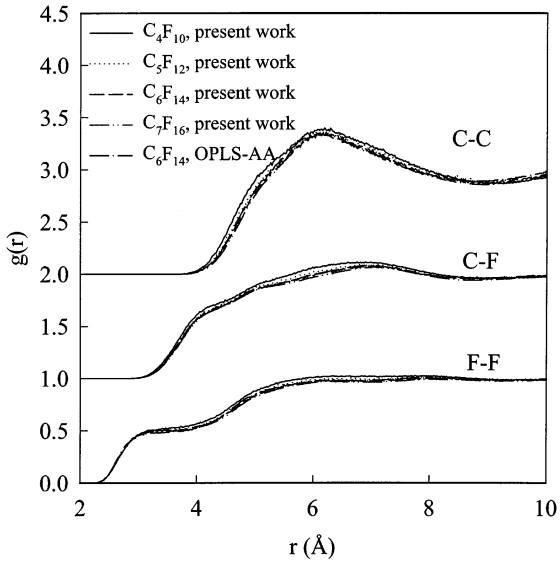

Figure 11. Intermolecular radial distribution functions for $C_4F_{10}-C_7F_{16}$ from MD simulations using the developed force field and for C_6F_{14} using the OPLS-AA force field at 298 K and 1 atm. (C−F and C−C intermolecular RDFs were offset by 1 and 2, respectively.)

is seen between MD simulation and X-ray measurements, indicating that F−F structure dominating the spectrum is correctly predicted by the developed force field. Both the experiment and MD simulations predict a shift of the first sharp diffraction peak (FSDP) to larger k values with decreasing temperature. This is consistent with the notion that the FSDP is a measure of intermolecular or interchain correlations. When temperature decreases, the density increases (see Table 8) and the average distance between the chain decreases. The width of the FSDP also decreases with decreasing temperature, indicative of an increasing order.

F. Pair Distribution Functions. Figure 11 shows the intermolecular RDF's for $C_4F_{10}-C_7F_{16}$ at 298 K. The C−C, C−F, and F−F intermolecular RDF's for C_4F_{10}, C_5F_{12}, C_6F_{14}, and C_7F_{16} are very similar to each other, with C_7F_{16} being systematically the lowest and C_4F_{10} being the highest as expected due to the largest molecular volume of C_7F_{16} and the smallest of C_4F_{10}. The C−C intermolecular RDF has a

pronounced first peak around 6.1 Å, the C−F intermolecular RDF has a very broad peak at 7 Å, and the F−F intermolecular RDF has a shoulder at about 3 Å and a peak smeared out from 6 to 8 Å. The insignificant changes in the intermolecular RDF's for C_4F_{10}−C_7F_{16} at 298 K indicates that PFA packing does not change considerably with an increase in molecular weight.

V. Comparison with the OPLS-AA Force Field

The OPLS-AA force field is the most recent PTFE force field published in the literature providing the most accurate description of densities and heats of vaporization for PFAs. Polymer properties such as characteristic ratio, torsional correlation times, and conformational populations have not been calculated for the OPLS-AA force field, leaving the applicability of the force field for prediction of polymer properties under question. We performed MD simulations at 298 K and 1 atm pressure for C_5F_{12} and C_6F_{14} and at 580 K and 1000 atm for $C_{20}F_{42}$ using the OPLS-AA force field to compare polymer properties yielded by the OPLS-AA force field with those from the developed force field and available experimental data where available. The same number of chains was used in simulations with the OPLS-AA force field as in the simulations with the developed force field. MD simulations code *Lucretius*[27] was modified to include only half of the nonbonded interactions for the intramolecular atomic pairs that are exactly three bonds away as required by the formulation of the OPLS-AA force field. Simulation methodology as described above was used, but the long-range electrostatic interactions were treated using the Ewald summation algorithm[43] with alpha 7.0 Å and the number of vectors for reciprocal space summation being 3^3. The length of MD simulations of C_5F_{12} was 5 ns and 20 ns for C_6F_{14} and $C_{20}F_{42}$.

A. Thermodynamics Properties. The OPLS-AA force field was reported to describe densities with 1% of an average unsigned error for CF_4−C_6F_{14}, comparable with the accuracy of the developed force field. However, it predicts the density of $C_{20}F_{42}$ at 580 K and 1000 atm about 1.5% higher than the experimental data, whereas the developed force field overestimates this density by 1.1%. The OPLS-AA force field, which included heat of vaporization data in its parametrization of the nonbonded interactions, described heats of vaporization with an average unsigned error of 3%, whereas the developed force field, which did not include heats of vaporization in its parametrization, predicted heats of vaporization about 10% higher than the experimental data.

B. Structural Properties. The intermolecular RDFs from MD simulations using the OPLS-AA force field compared with those MD simulations using the developed force field are shown in Figure 11. All C−C, C−F, and F−F RDFs are very similar between the two force fields, indicating that intermolecular packing is also similar between the two force fields. The total RDFs, with atoms connected by bonds and bends excluded for clarity, are shown in Figure 12. The differences in the peak positions of RDFs are due to different intramolecular structure and are attributed to the differences between the equilibrium bond lengths for the C−C bond of about 3% as well as differences in equilibrium bend angles and torsional populations yielded by the two potentials. In the developed potential, the equilibrium bond length and bend angles were fitted to reproduce equilibrium geometries of C_4F_{10} and C_5F_{12}, whereas generic values were used in the OPLS-AA force field, possibly giving rise to differences in intramolecular structure between two force fields.

C. Conformational Populations. Relative conformational energetics from the general OPLS-AA force field for C_4F_{10}, C_5F_{12}, and C_6F_{14} drives are shown in Figures 1−3. The general OPLS-AA force field clearly does not predict a stable ortho conformer and overestimates the g ↔ a barrier. It also has a systematically higher gauche energy than the developed force field. Even the specific OPLS-AA force fields for C_4F_{10} and C_5F_{12} do not predict a stable ortho conformers; see Watkins el al.[10] Figure 2b demonstrates that generally the OPLS-AA force field does not predict a stable gg conformer for C_5F_{12}. These shortcomings of the OPLS-AA force field will lead to the quite different structural and dynamic properties of PTFE oligomers from those predicted by the developed force field, which is capable of adequately describing the conformational energetics of C_4F_{10}−C_6F_{14}.

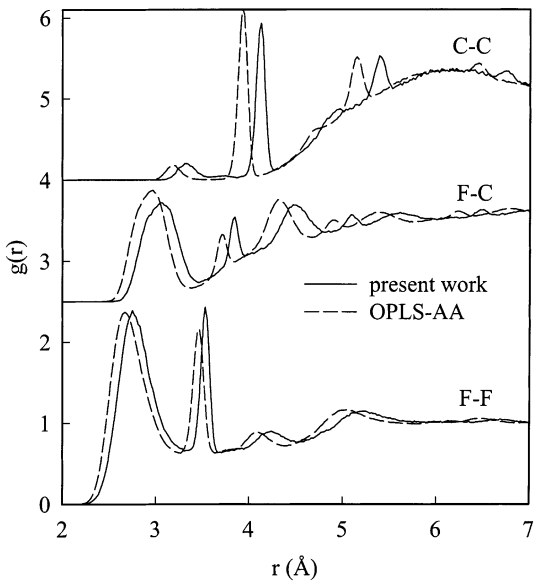

Figure 12. Radial distribution functions for C_6F_{14} at 298 K and 1 atm with the contributions from atoms connected by bonds and bends excluded. (C−F and C−C intermolecular RDFs were offset by 2.5 and 4, respectively.)

Conformational populations of C_6F_{14} around the C−C−C−C bond are compared between the two force fields in Figure 8. Higher anti population, the absence of a stable ortho state, and a lower gauche population predicted by the OPLS-AA force field compared to the developed force field are due to inability of the OPLS-AA potential to describe conformational energetics of the PTFE oligomers shown in Figures 1−3. The total gauche (+ortho) population of 7.2% for C_6F_{14} at 298 K shown in Table 9 is also much lower than the values 19−24% obtained from the analysis of D-LAM Raman bands of liquid PFA from C_9F_{20} to $C_{20}F_{42}$ at 300 K,[34] whereas the developed force field yields values of 15−18%, which are in much better agreement with the experiments.[34]

As described above for the developed force field, C_∞ of PTFE at 600 K was determined from a six-state RIS model parametrized to reproduce the populations, dihedral angles, and valence angles obtained from simulations of C_5F_{12} using the OPLS-AA force field. Here, a zero population for the ortho states reduces the model to a four-state RIS model. The RIS model was found to accurately reproduce the average end-to-end distance of $C_{20}F_{42}$ from MD simulations at 580 K. A value of $C_\infty = 28$ was obtained from the OPLS-AA based RIS model compared to $C_\infty = 15$ for the developed force field and 8 ± 2.5 from the light scattering experiments.[36] This significant increase in chain dimensions is consistent with the very low gauche (+ortho) population yielded by the OPLS-AA force field.

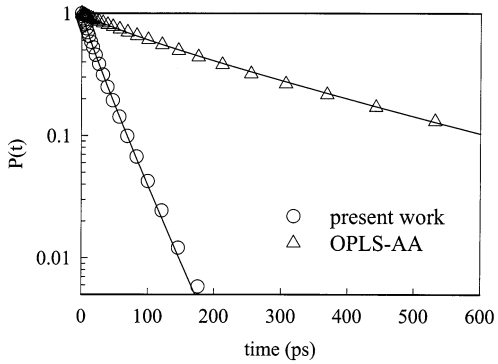

Figure 13. Torsional ACF $P(t)$ for the C−C−C−C angle for C_6F_{14} at 298 K and 1 atm.

D. Dynamics and Transport Properties. Conformational dynamics is important for polymer transport properties as polymer motion in bulk occurs by means of torsional transitions. The torsional autocorrelation function (TACF) is a measure of time it takes a given torsion to decorrelate from its position and reflects torsional dynamics. The TACF was determined using the relationship

$$P_i(t) = \frac{\langle \cos(\phi_i(t)) \cos(\phi_i(0)) \rangle - \langle \cos(\phi_i(0)) \rangle^2}{\langle \cos^2(\phi_i(0)) \rangle - \langle \cos(\phi_i(0)) \rangle^2} \qquad (10)$$

where the subscript indicates the dihedral type and $\phi_i(t)$ is the dihedral angle at time t. The TACF for the C−C−C−C torsional types for C_6F_{14} is shown in Figure 13. The C−C−C−C TACF decays much slower for the OPLS-AA force field than for the developed force field. The torsional autocorrelation time defined as the area under the TACF curve is 28.7 ps for the developed force field and 248 ps for the OPLS-AA force field, indicating that torsional dynamics of PTFE predicted by the OPLS-AA force field is an order of magnitude slower than the one predicted by the developed force field. It is one of the largest differences between two force fields and is expected to significantly affect high molecular weight PTFE dynamics. The slow dynamics from the OPLS-AA force field compared to that from the developed force field is due to a much higher g ↔ a barrier in the OPLS-AA force field.

The viscosity of C_6F_{14} predicted by the OPLS-AA force field shown in Figure 9 is lower than the value predicted by the developed force field. In agreement with the viscosity results, the C_6F_{14} center of mass translational diffusion coefficient D_{C6F14}(OPLS-AA) $= 0.155 \times 10^{-8}$ m^2/s, which is about 30% faster than D_{C6F14}(developed FF) $= 0.12 \times 10^{-8}$ m^2/s. The diffusion coefficient of PFA from the OPLS-AA force field is higher than the one from the developed force field despite the much slower conformational dynamics from the analysis of TACF for the OPLS-AA force field. This is due to the insensitivity of transport properties of low molecular weight oligomers on conformational dynamics. For high molecular weight PTFE, however, we expect polymer transport from the OPLS-AA force field to be much slower than the one predicted by the developed force field, as polymer motion occurs by conformational relaxation.

VI. Conclusions

A new ab initio quantum chemistry based classical force field for MD simulations of PTFE was developed by fitting conformational energetics and geometries of C_4F_{10} and C_5F_{12}. The transferability of the torsional potential to longer perfluoroalkanes was tested by comparing conformational energetics of C_6F_{14} from ab initio quantum chemistry with that predicted by the force field. The repulsion parameters were determined by fitting the Hartree−Fock complex energy for $CF_4\cdots CF_4$, whereas the dispersion parameters were determined from the London formula and scaled to match the experimental density of C_7F_{16} at 298 K and 1 atm. This force field predicted densities of various PTFE oligomers from C_4F_{10} to $C_{20}F_{42}$ at temperatures from 200 to 580 K within an average error of 1% and a maximum error of 2.2%. The predicted heats of vaporization were approximately 10% above experimental values. An excellent agreement was seen between the experimentally measured X-ray structure factor and that predicted by MD simulations for C_9F_{20} at 377 and 295 K. The force field predicted conformational populations in good agreement with analysis of D-LAM spectra. The characteristic ratio of PTFE at 600 K was predicted on the basis of MD simulations of $C_{20}F_{42}$ with the rotational isometric state model molecular weight correction. The developed force field yielded a characteristic ratio of 15, somewhat higher than the value of 8 ± 2.5 from the light scattering experiments. Viscosity of PTFE oligomers at 298 K from MD simulations was in good agreement with the available experimental data.

The OPLS-AA force field yielded accurate thermodynamic data (density, heat of vaporization) and a good viscosity for C_6F_{14}. However, it predicts a fraction of gauche(+ortho) conformers 2 times less than the one from analysis of D-LAM spectra and a characteristic ratio of 28, much larger than the experimental value of 8 ± 2.5 from the light scattering experiments, showing the inability of the OPLS-AA to predict polymer conformational properties. Moreover, the ortho conformer is not stable according to the OPLS-AA force field, whereas the force field developed in this paper predicts a stable ortho conformer in agreement with ab initio quantum chemistry calculations.

Finally, we would like to emphasize the importance of accurate description of relative conformational energies of the low-energy conformers and barriers between them on polymer static and dynamic properties. For example, overestimation of the gauche energy and the absence of the ortho state in the OPLS-AA force field led to a significant overestimation of polymer dimension (characteristic ratio of 28), whereas overestimation of the barrier heights resulted in conformation dynamics 1 order of magnitude slower than the one predicted by the developed force filed, which correctly describes the conformational energetics. Therefore, we would recommend use of the developed force field for studies of the structural and dynamic properties of PTFE melts rather than the OPLS-AA force field.

Acknowledgment. O.B. acknowledges funding through the Department of Energy, Sandia National Laboratory, Contract No. 18872, and thanks Gary Grest (Sandia National Laboratory) for his collaboration on this project.

References and Notes

(1) *Fluoropolymers 2: Properties*; Hougham, et al., Ed.; Plenum Press: New York, 1999.

(2) Kajdas, C. Industrial Lubricants. In *Chemistry and Technology of Lubricants*; Mortier, R. M., Orszulik, S. T., Ed.; VCH Publishers, Inc.: New York, 1992.

(3) Eastoe, J.; Bayazit, Z.; Martel, S.; Steytler, D. C.; Heenan, R. K. *Langmuir* **1996**, *12*, 1423.

(4) Ogino, K.; Abe, M. *Mixed Surfactant Systems*; M. Dekker, Inc.; New York, 1993.

(5) Eger, E. I., II; Jonescu, P.; Laster, M. J.; Gong, D.; Hudlicky, T.; Kending, J. J.; Harris, A.; Trudell, J. R.; Pohorille, A. *Anesth. Analg*. **1999**, *88*, 867.

(6) Holt, D.; Farmer, B. L. *Fluoropolymers 2: Properties*; Hougham, et al., Ed.; Plenum Press: New York, 1999.

(7) Cui, S. T.; Siepmann, J. I.; Cochran, H. D.; Cummings, P. T. *Fluid Phase Equilib.* **1998**, *146*, 51.

(8) Röthlisberger, U.; Laasonen, K.; Klein, M. L.; Sprik, M. *J. Chem. Phys.* **1996**, *104*, 3692.

(9) Sprik, M.; Röthlisberger, U.; Klein, M. L. *Mol. Phys.* **1999**, *97*, 355.

(10) Watkins, E. K.; Jorgensen, W. L. *J. Phys. Chem. A* **2001**, *105*, 4118.

(11) McCabe, C.; Cummings, P. T. Private communication.

(12) Smith G. D.; Borodin, O.; Pekny, M.; Annis, B.; Londono, D.; Jaffe. R. *Spectrochim. Acta, Part A* **1997**, *53*, 1273.

(13) Smith, G. D.; Jaffe, R. L.; Yoon, D. Y. *Macromolecules* **1994**, *27*, 3166.

(14) Albinsson, B.; Milch, J. *J. Phys. Chem*. **1996**, *100*, 3418.

(15) Dunning, T. H. *J. Chem. Phys.* **1987**, *98*, 1007.

(16) Krishman, R.; Binkley, J. S.; Seeger, R.; Pople, J. A. *J. Chem. Phys.* **1980**, *72*, 650.

(17) Kendall, R. A.; Dunning, T. H., Jr.; Harrison, R. J. *J. Chem. Phys.* **1996**, *96*, 6796.

(18) Becke, A. D. *J. Chem. Phys*. **1993**, *98*, 5648. Lee, C.; Yang, W.; Parr, R. G. *Phys. Rev. B*, **1988**, *37*, 785.

(19) Borodin, O.; Smith, G. D. Manuscript in preparation.

(20) Frisch, M. J.; Trucks, G. W.; Schlegel, H. B.; Scuseria, G. E.; Robb, M. A.; Cheeseman, J. R.; Zakrzewski, V. G.; Montgomery, J. A., Jr.; Stratmann, R. E.; Burant, J. C.; Dapprich, S.; Millam, J. M.; Daniels, A. D.; Kudin, K. N.; Strain, M. C.; Farkas, O.; Tomasi, J.; Barone, V.; Cossi, M.; Cammi, R.; Mennucci, B.; Pomelli, C.; Adamo, C.; Clifford, S.; Ochterski, J.; Petersson, G. A.; Ayala, P. Y.; Cui, Q.; Morokuma, K.; Malick, D. K.; Rabuck, A. D.; Raghavachari, K.; Foresman, J. B.; Cioslowski, J.; Ortiz, J. V.; Stefanov, B. B.; Liu, G.; Liashenko, A.; Piskorz, P.; Komaromi, I.; Gomperts, R.; Martin, R. L.; Fox, D. J.; Keith, T.; Al-Laham, M. A.; Peng, C. Y.; Nanayakkara, A.; Gonzalez, C.; Challacombe, M.; Gill, P. M. W.; Johnson, B. G.; Chen, W.; Wong, M. W.; Andres, J. L.; Head-Gordon, M.; Replogle, E. S.; Pople, J. A. *Gaussian 98*, revision A.7; Gaussian, Inc.: Pittsburgh, PA, 1998.

(21) Stone, A. J. *The Theory of Intermolecular Forces*; Oxford University Press: New York, 1996.

(22) van Duijneveldt, F. B.; van Duijneveldt-van de Rijdt, J. G. C. M.; van Lenthe, J. H. *Chem. Rev.* **1994**, *94*, 1873.

(23) Smith, G. D.; Jaffe, R. L.; Yoon, D. Y. *J. Phys. Chem.* **1993**, *97*, 298.

(24) Byutner, O. G.; Smith, G. D. *Macromolecules* **2000**, *33*, 4264.

(25) Sorensen, R. A.; Liau, W. B.; Kesner, L.; Boyd, R. H. *Macromolecules* **1988**, *21*, 200.

(26) *CRC Handbook*, 81st ed.; CRC Press: Boca Raton, FL, 2000.

(27) Lucretius, MD simulations code, http://www.che.utah.edu/~gd-smith/mdcode/main.html.

(28) Nose, S. In *Computer Simulation in Materials Science*; Meyer, M., Pontikis, V., Eds.; Kluwer Academic Publishers: Dordrecht, Netherlands, 1991; p 21.

(29) Martyna, G. J., Tuckerman, M.; Tobias, D. J.; Klein, M. L. *Mol. Phys.* **1996**, *87*, 1117.

(30) Smith, G. D.; Jaffe, R. L.; Yoon, D. Y. *Macromolecules* **1993**, *26*, 6, 298.

(31) Ryckaert, J. P.; Ciccotti, G.; Berendsen, H. J. C. *J. Comput. Phys.* **1977**, *23*, 327.

(32) Palmer, B. J. *J. Comput. Phys.* **1993**, *104*, 470.

(33) Dee, G. T.; Sauer, B. B.; Haley, B. J. *Macromolecules* **1994**, *27*, 6106.

(34) Snyder, R. G. *J. Chem. Phys.* **1982**, *76*, 3921.

(35) Smith, G. D.; Jaffe, R. L.; Yoon, D. Y. *Macromolecules* **1994**, *27*, 3166.

(36) Chu, B.; Wu, C.; Buck, W. *Macromolecules* **1989**, *22*, 831.

(37) Harkins, D. *Evaluation of Available Perfluorobutane Data for Selected Physical Properties*; Oak Ridge Gaseous Diffusion Plant: Oak Ridge, TN, 1990.

(38) Burger, L. L.; Cady, G. H. *J. Am. Chem. Soc.* **1951**, *73*, 4243.

(39) Stiles, V. E.; Cady, G. H. *J. Am. Chem. Soc.* **1952**, *74*, 3771.

(40) Grosse, A. V.; Cady, G. H. *Ind. Eng. Chem*. **1947**, *39*, 367.

(41) Haile, J. M. *Molecular Dynamics Simulations*; Wiley: New York, 1992.

(42) Habenschuss, A.; Londono, J. D.; Kim, M.-H. Manuscript in preparation.

(43) Allen, M. P.; Tildesley, D. J. *Computer Simulation of Liquids*; Oxford University Press: New York, 1987.